Ring Resonators With Vertically Coupling Grating for Densely Multiplexed Applications

Sam Werquin, Yannick De Koninck, and Peter Bienstman

***Abstract*— Silicon-on-insulator photonic microring resonators are ideal components for applications that require a high degree of multiplexing because of their small size. However, when very high numbers of microrings are used in parallel, grating couplers and waveguide routing quickly take up more chip space than the actual rings. Therefore, we suggest to combine microring resonators with local weak gratings to read out light directly from the microring while still maintaining high-quality factors of 19 000. We demonstrate simulation results and an experimental analysis of different grating parameters. The resonance spectrum is recovered from the vertical emission of the microring grating, without using a traditional output waveguide.**

***Index Terms*— Microring resonator, grating, vertical coupling.**

I. Introduction

SILICON-ON-INSULATOR (SOI) photonic microring resonators have proven to be excellent components for a variety of integrated applications such as photonic biosensing [1], [2] or all-optical filters in telecommunications [3]. For sensing applications in particular, an important asset of microring resonators is their small size and their ability to perform multiplexed assays [4]. Vertical grating couplers and waveguides are used to couple light in and out of the chip and to address the actual sensors. For low levels of multiplexing, this is an adequate solution. However, next-generation applications like DNA sequencing [5] can require thousands of detections in parallel. Microring sensors have proven successful for multiplexed DNA detection [6], but the access waveguides pose problems in applications with massive parallelization. For such high levels of multiplexing, the waveguide routing on the chip surface quickly becomes impossible as waveguides start to take up more chip space than the actual sensors. Therefore, we suggest to combine a microring resonator with a weak grating. The combination of microrings with gratings has been investigated for different applications [7], [8]. We suggest a technique that enables direct interrogation of the microring resonance, without the need for output waveguides and output grating couplers, similar to the one adopted in [9]. However, by adopting a weak grating approach, the resonance maintains a much higher quality factor, which is of the utmost importance for most applications. Compared to the sensor array presented in [4], a microring with a weak grating to replace the access waveguides can save up to 0.1 mm^2 of chip footprint. In this letter, we present a proof-of-principle demonstration of direct vertical read-out of a microring resonator, supported by simulation results.

Manuscript received August 22, 2014; revised September 18, 2014; accepted October 9, 2014. Date of publication October 13, 2014; date of current version December 8, 2014. This work was supported by the Special Research Fund of Ghent University (BOF UGent).

The authors are with the Center for Nano- and Biophotonics, Department of Information Technology, Ghent University, Ghent 9000, Belgium, and also with imec, Leuven 3001, Belgium (e-mail: sam.werquin@intec.ugent.be; yannick.dekoninck@intec.ugent.be; peter.bienstman@ugent.be).

Color versions of one or more of the figures in this letter are available online at http://ieeexplore.ieee.org.

Digital Object Identifier 10.1109/LPT.2014.2362844

II. Ring Design

For this purpose, we have designed microring resonators combined with a weak grating that couples light directly out of the ring. The microring consist of a 450 nm wide waveguide. The grating is created by etching slits in the silicon top layer of 220 nm until the buried oxide layer is reached, and is defined in the same lithographical step as the microring resonator. The weak grating effect is obtained by spatially separating the grating region from the silicon waveguide. This way only the evanescent tail of the waveguide mode interacts with the grating and we can assume a weak interaction between both. The fill factor of the grating is 50% and a period of 547 nm is determined to diffract light from the waveguide in the vertical direction using the Bragg condition. A Scanning Electron Micrograph (SEM) of the microring resonator with weak grating on both sides of the waveguide is shown in fig. 1. The inset shows a magnification of the grating region. For this proof-of-principle demonstration, we use microrings in the all-pass configuration for easy characterization of different grating parameters on an vertical fiber setup. The weak gratings are located in the vicinity of the ring waveguide on the opposite side of the ring compared to the coupling waveguide. The grating functions as a drop port for the microring and diffracts light upward, where it can be collected by a camera. Simulations are performed to estimate the effect on the quality of the ring resonance for different grating configurations and to visualize the dropped light through the weak grating. Devices on SOI chips are fabricated in a complementary metal-oxide-semiconductor (CMOS) pilot line [10] for experimental characterization.

III. Simulations

The microring resonators combined with weak gratings are simulated using the three-dimensional finite-difference time-domain (3D-FDTD) simulation tool Meep3D [11], [12]. For these simulations, a simple model of a silicon wire microring with 5 μm radius on a buried oxide layer with air as a top cladding is used. The very high index contrast allows

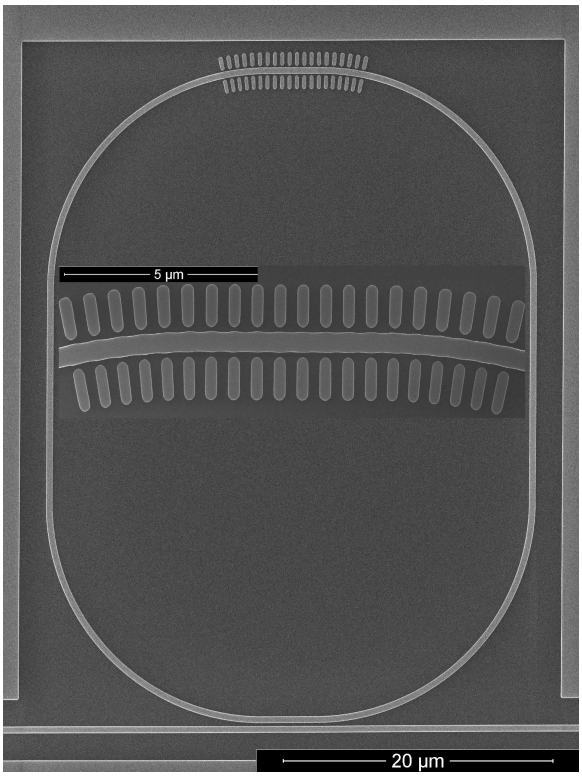

Fig. 1. SEM-picture of the microring resonator with weak grating in the vicinity of the waveguide. The inset shows a magnification of the grating region.

us to limit the device dimensions which significantly reduces simulation time. We use Harminv [13], [14] to perform a harmonic inversion of the time-dependent field values recorded in the resonator to determine the quality factor of the different resonator modes. By comparing the simulation results to the reference microring without grating, the influence of the weak grating on the resonator mode and the grating-associated losses can be extracted. We have simulated the microring with weak grating for different grating lengths and different gaps between waveguide and grating. The influence of a weak grating on both sides of the ring waveguide has also been investigated. The grating loss A_{gr}, which is in fact the only extra loss mechanism after taking into account the reference ring simulation, is defined as $A_{gr} = 1 - \exp(-\alpha_{gr} L)$, with α_{gr} the attenuation coefficient associated with the grating. α_{gr} can be determined from the simulated quality factors by using relation (1).

$$\frac{1}{Q} = \frac{1}{Q_{ref}} + \frac{1}{Q_{gr}} \quad \text{and} \quad \frac{\omega}{Q} = \frac{\alpha c}{n_g} \tag{1}$$

Here, Q is the simulated quality factor of the microring with grating while Q_{ref} corresponds to the reference situation. ω and n_g are the angular frequency and the group index of the resonator mode, respectively. These results are summarized in fig. 2. The simulations show a significant effect of the weak grating on the resonator losses, while still maintaining a reasonable quality factor. For a spacing between grating and waveguide of 120 nm, the simulations show the ring losses are increasing linearly with increasing grating length.

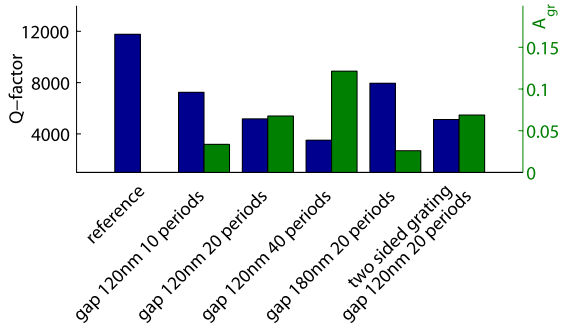

Fig. 2. Simulated quality factors and grating associated losses for microring resonators with different grating configurations.

When the spacing is increased to 180 nm, the resonator losses are significantly reduced, as can be expected by the reduced overlap between the waveguide mode and the grating. If a two sided grating is used, with second grating placed at the inner radius of the bend in an attempt to increase the outcoupling, we notice only very limited extra losses. This can be explained by the fact that the mode is concentrated at the outer edge of the waveguide in the bend sections. Additional simulations show very little effect on the simulated losses for a change in grating period of 30 nm. Also, in general for a fixed period, the grating loss increases with increasing wavelength. This can most likely be attributed to the reduced confinement of the waveguide mode for larger wavelengths, rather than a wavelength dependency of the grating losses. The grating period does determine the diffraction angle of the grating though.

Using a commercial-grade simulator based on the finite-difference time-domain method [15], the far-field response of the grating is simulated. The resulting projection on the hemisphere 1 m above a two-sided grating with gap 120 nm and 20 periods of 547 nm is plotted in fig. 3. The figure shows the intensities of the optical field for the different directions (θ, ϕ), with the propagation of the counter clockwise mode in the waveguide along the negative x direction, or $\phi = 180°$. The majority of the light is emitted in the $\phi = 0°$ direction, at a polar angle θ of approximately 30° from the surface normal. The opening angle along the azimuthal ϕ direction is approximately 60°, which is expected for diffraction from a 450 nm wide waveguide.

IV. Experiments

For the experimental characterization of the microrings with weak gratings, the devices are clad with silicon oxide. This cladding material approaches the index contrast of a water cladding which will most likely be used in a biomedical sensing application. The microrings consist of silicon wire waveguides of 450 nm with 16 μm bends. The directional coupler with the pass waveguide has a gap of 250 nm and 4 μm straight arms. The microrings with gratings are measured in the pass configuration on a vertical fiber setup. An Agilent 81980A tunable laser is swept over a wavelength range of 60 nm and an Agilent 81635A optical powermeter records the optical power with 1 pm wavelength resolution. The resulting

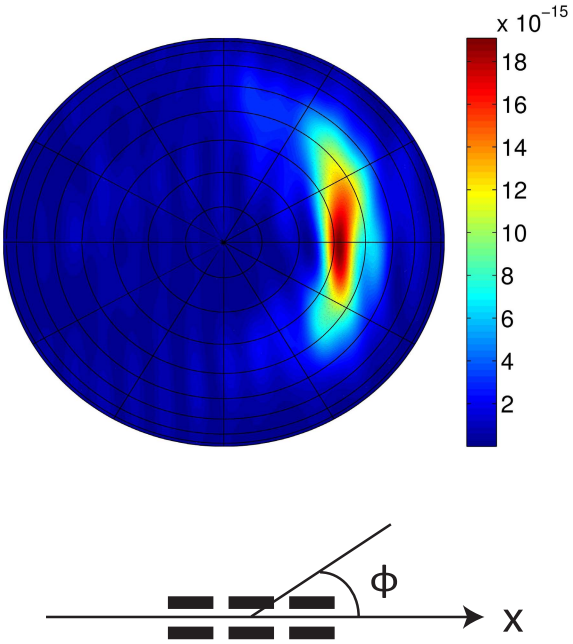

Fig. 3. Simulated far-field response on the hemisphere above the grating. The center of the grating coincides with the origin of the coordinate system, as indicated by the schematic top view. Concentric circles represent increments of 10° in the polar angle θ, while radial lines correspond to steps of 30° in the azimuthal angle ϕ. The highest intensity optical field is found around the direction $\theta = 30°, \phi = 0°$.

microring spectra can be used to extract resonance characteristics for different grating configurations such as quality factor and losses by fitting a lorentzian lineshape to the resonance dips. To monitor the microring directly by recording the light vertically diffracted by the grating, an image of the integrated chip with microring resonators is recorded by a Xenics Xeva-1.7-320 infrared camera mounted on a magnifying objective. In correspondence with the simulated far-field response, the camera is mounted under an angle of 30° to pick up the grating emission.

A. Power Transmission

The round-trip and coupling loss of the microring resonances can be extracted from the parameters of the lorentzian approximation for the transmission (2).

$$T = \frac{a^2 - 2ar\cos(\phi) + r^2}{1 - 2ar\cos(\phi) + (ar)^2} \tag{2}$$

Round-trip loss for a microring resonator with attenuation coefficient α and round-trip length L is represented by the amplitude reduction coefficient $a = \exp(-\alpha L)$, while ϕ equals the round-trip phase change. The directional coupler amplitude self-coupling coefficient $r = \sqrt{1 - k^2}$ represents the coupling losses corresponding to a field coupling coefficient k. The method described in [16] returns a set (a,r) and by comparing the behaviour of the solutions for different devices, the trends in a and r can be identified. The resulting a and r of the microring resonators with a weak grating are given in fig. 4 as a function of wavelength for different grating lengths. The results in the graph are for a grating-to-waveguide gap of

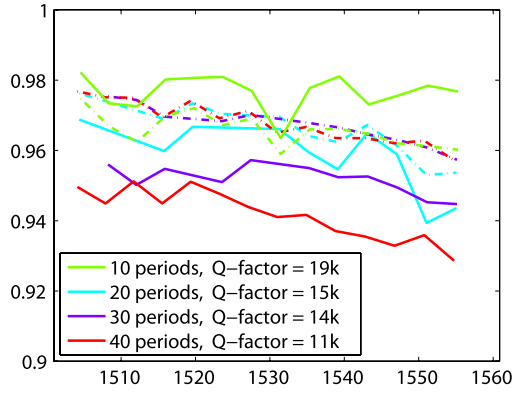

Fig. 4. Device and wavelength dependent coupling and round-trip loss for microrings with different number of weak grating periods. Dashed lines represent the coupling coefficient r while the full lines show the round-trip amplitude reduction coefficient a. The weak grating periods are 547 nm with 50% filling factor while the waveguide-grating gap is 130 nm.

130 nm and a grating period of 547 nm with 50% filling factor. The quality factors of the resonances around 1550 nm are indicated in the legend.

The method in [16] can not distinguish between a and r, but since the dashed lines do not vary for different grating lengths, they have to correspond to the coupling coefficients. The full lines represent round-trip losses that increase with increasing grating length, which is in good agreement with the simulation results. Broadening of some resonances by resonance splitting results in poorly-fit parameters which causes the particularities in the graph. In general, round-trip and coupling losses increase slightly with increasing wavelength. Changing the period of the fabricated grating does not result in changes in the recorded losses of the resonator mode. For a gap of 200 nm, increasing the grating length no longer has any effect on the losses of the microring resonance. This indicates the grating has only a very limited effect for such large gaps. The quality factor recorded for a resonance around 1550 is 23000 for a gap of 200 nm and 20 grating periods of 547 nm, which is indeed significantly higher than the quality factor of 15000 reported in fig. 4 for a 130 nm gap.

B. Grating Image

Fig. 5 shows the image of the microring with weak grating on resonance as recorded by an infrared camera under an angle of 30°. The microring grating is imaged on the camera array as a bright spot with some low intensity fringes due to focusing issues. The power integrated over the spot size can be used as a transmission characteristic of the microring. Compared to the scattering from the waveguide edges, the power diffracted by the grating is two orders of magnitude higher. By sweeping a Tunics Plus CL tunable laser and recording the transmission at every wavelength, a spectral response of the microring is obtained. This is represented in fig. 6. A lorentzian shape can be fitted to the microring spectrum to obtain the resonance parameters. This results in a resonance quality factor of 20000 at a wavelength of 1523.5 nm, which corresponds very well to the quality factor of 19000 that we obtain for the same resonance by investigating the pass transmission

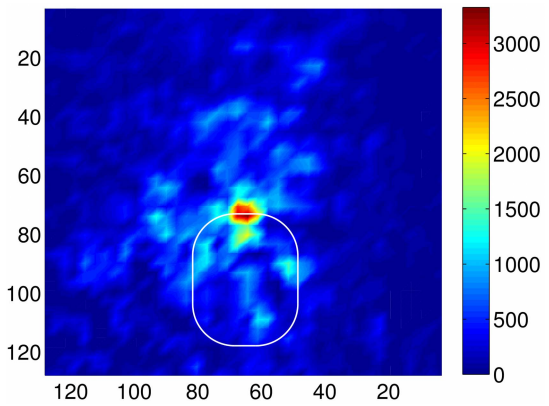

Fig. 5. Schematic microring and weak grating image as recorded by an infrared camera picking up the emission at 30°. Axes are expressed in μm. The color scale represents the counts per individual pixel.

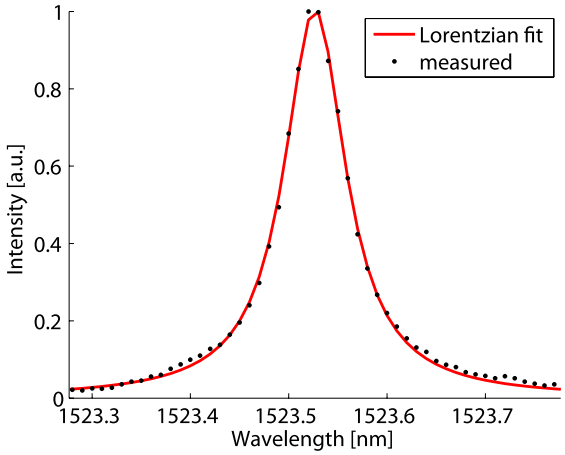

Fig. 6. Microring spectrum and resulting lorentzian fit obtained by recording the near-vertical emission of the grating using an infrared camera.

on the vertical fiber setup. This indicates the transmission of the weak grating represents the same resonance of the microring and confirms the ability to record the microring resonance without using an output waveguide.

V. Conclusion

We have simulated and experimentally characterized the combination of a microring resonator with a weak grating for direct interrogation of the microring. The effect of different grating parameters is evaluated. Both simulation and experiment show near-vertical emission from a microring can be achieved, while still maintaining high qualilty factors of 19000. Using an infrared camera to collect the vertically radiated light, the resonance spectrum is recovered. In future work, the use of similar gratings to couple light both in and out of the microring can be investigated.

References

[1] M. Iqbal *et al.*, "Label-free biosensor arrays based on silicon ring resonators and high-speed optical scanning instrumentation," *IEEE J. Sel. Topics Quantum Electron.*, vol. 16, no. 3, pp. 654–661, May/Jun. 2010.

[2] A. J. Qavi and R. C. Bailey, "Multiplexed detection and label-free quantitation of microRNAs using arrays of silicon photonic microring resonators," *Angew. Chem. Int. Ed.*, vol. 49, no. 27, pp. 4608–4611, Jun. 2010.

[3] P. De Heyn, J. Luo, S. Di Lucente, N. Calabretta, H. J. S. Dorren, and D. Van Thourhout, "In-band label extractor based on cascaded Si ring resonators enabling 160 Gb/s optical packet switching modules," *J. Lightw. Technol.*, vol. 32, no. 9, pp. 1647–1653, May 1, 2014.

[4] K. De Vos *et al.*, "Multiplexed antibody detection with an array of silicon-on-insulator microring resonators," *IEEE Photon. J.*, vol. 1, no. 4, pp. 225–235, Oct. 2009.

[5] T. T. Torres, M. Metta, B. Ottenwälder, and C. Schlötterer, "Gene expression profiling by massively parallel sequencing," *Genome Res.*, vol. 18, no. 1, pp. 172–177, Jan. 2008.

[6] A. J. Qavi, T. M. Mysz, and R. C. Bailey, "Isothermal discrimination of single-nucleotide polymorphisms via real-time kinetic desorption and label-free detection of DNA using silicon photonic microring resonator arrays," *Anal. Chem.*, vol. 83, no. 17, pp. 6827–6833, Sep. 2011.

[7] A. Samarelli *et al.*, "Grating-assisted micro-ring resonators for silicon dual mode filters," in *CLEO EUROPE/EQEC Conf. Dig.*, May 2011, p. 1.

[8] S. Iijima, Y. Ohtera, and H. Yamada, "High-Q microdisk resonator having sub-wavelength grating on its sidewall," in *Proc. Conf. Lasers Electro-Opt. Pacific Rim (CLEO-PR)*, Jun./Jul. 2013, pp. 1–2.

[9] C. Qiu and Q. Xu, "Controlling normal incident optical waves with an integrated resonator," *Opt. Exp.*, vol. 19, no. 27, pp. 26905–26910, Dec. 2011.

[10] (2014). *ePIXfab, The Silicon Photonics Platform*. [Online]. Available: http://www.epixfab.eu/

[11] A. F. Oskooi, D. Roundy, M. Ibanescu, P. Bermel, J. D. Joannopoulos, and S. G. Johnson, "MEEP: A flexible free-software package for electromagnetic simulations by the FDTD method," *Comput. Phys. Commun.*, vol. 181, no. 3, pp. 687–702, Mar. 2010.

[12] (2014). *The IPKISS Parametric Design Framework*. [Online]. Available: http://www.ipkiss.org

[13] (2006). *Harminv*. [Online]. Available: http://ab-initio.mit.edu/wiki/index.php/Harminv

[14] H. S. Taylor and V. A. Mandelshtam, "Harmonic inversion of time signals and its applications," *J. Chem. Phys.*, vol. 107, no. 17, pp. 6756–6769, 1997.

[15] Lumerical Solutions Inc. (2014). [Online]. Available: http://www.lumerical.com/tcad-products/fdtd/

[16] W. R. McKinnon *et al.*, "Extracting coupling and loss coefficients from a ring resonator," *Opt. Exp.*, vol. 17, no. 21, pp. 18971–18982, Oct. 2009.